Pergamon

0045-7949(94)00573-7

Computers & Structures Vol. 56, No. 6, pp. 1019–1028, 1995

0045-7949/95 $9.50 + 0.00

FINITE ELEMENTS FOR POST-BUCKLING ANALYSIS. II—APPLICATION TO COMPOSITE PLATE ASSEMBLIES

E. J. Barbero, I. G. Raftoyiannis and **L. A. Godoy**

Mechanical and Aerospace Engineering, Constructed Facilities Center, West Virginia University, Morgantown, WV 26506-6106, U.S.A.

(*Received* 3 *February* 1994)

Abstract—In a companion paper the authors presented a convenient formulation for the stability analysis of structures using the finite element method. The main assumptions are linear elasticity, a linear fundamental path and the existence of distinct critical loads. The formulation developed is known as the W-formulation, where the energy is written in terms of a sliding set of incremental coordinates measured with respect to the fundamental path. In the present paper a number of applications of finite elements for post-buckling analysis on composite plate assemblies are presented. Thin-walled composite plates, I-beams, angle sections, and a specially designed box-beam with flanges (unicolumn) are studied in post-buckling when axially loaded. The results are in good agreement with previous studies. Moreover, a parametric study involving critical buckling load and geometry is presented for the case of the unicolumn.

1. INTRODUCTION

In a companion paper [1], the authors presented a finite element formulation suitable for stability analysis following the general theory of elastic stability. This means that finite elements are employed to obtain the total potential energy of the system and the derivatives required to evaluate a critical state along a linear fundamental path, to investigate the nature of such a critical state, and to obtain the initial post critical path. One of the advantages of the technique is that the matrices usually employed in finite element analysis are the only ingredients necessary to carry out the calculations mentioned above. The particular energy formulation adopted in part I is the so-called W-formulation, in which the fundamental path is first obtained and substituted into the energy. This new expression of the energy is thus obtained in terms of incremental coordinates [2] measured with respect to the fundamental path.

Previous applications of finite element analysis in the context of stability theory may be traced to the work of Walker [3]. A review of the applications to shells of revolution may be found in Flores and Godoy [4]. The post-buckling solution of plate assemblies has been tackled in the literature using finite strip methods (for an example see Ref. [5]). The purpose of this paper is to apply the finite element formulation to the analysis of the plate assemblies made of composite materials.

The first work known to the authors to use finite strips for the perturbation analysis of the post buckling path is that of Graves Smith and Sridharan [6]; they considered isotropic prismatic structures subjected to end compression. Problems of compatibility of displacements along the corners of the junctions between plates are discussed in Ref. [7]. Translations of the junctions in the cross sectional plane is investigated in [8]; while non-uniform compression was incorporated in [9]. In all cases mentioned, the material was assumed as isotropic, somehow reflecting an interest in steel or aluminum structural components. Linearized buckling of long plates made of composite materials was presented by Zeggane and Sridharan [10, 11] using Reissner–Mindlin infinite strips. A review of buckling of shear deformable, laminated, rectangular, anisotropic plates may be found in Ref. [12]. An extension of the finite strip approach to post buckling of composite cylindrical shells is in Ref. [13].

In the present work the finite element rather than the finite strip method is employed. With the increased capacity of present day workstations and personal computers, it is now possible to solve large problems without having to assume analytical approximations for prismatic members. Furthermore, the finite element methods easily allow the modelling of non-prismatic problems, complex boundary conditions and geometries.

2. DISPLACEMENTS AND DEFORMATIONS OF THE PLATES

The reference system and displacement field is identified in Fig. 1. Following a first order shear deformation theory, the displacement field is

$$\begin{aligned} u(x,y,z) &= u_0(x,y) - z\theta_x \\ v(x,y,z) &= v_0(x,y) - z\theta_y \\ w(x,y,z) &= w_0(x,y) \end{aligned} \qquad (1)$$

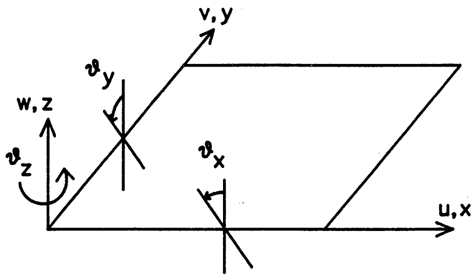

Fig. 1. Reference system and displacement field.

where θ_x and θ_y are the average rotations of a line initially perpendicular to the longitudinal plane. Within each element these displacements can be expressed with respect to nodal unknowns with the aid of the shape functions N_i as

$$u=\sum_{i=1}^{N} N_i u_i,\quad v=\sum_{i=1}^{N} N_i v_i,\quad w=\sum_{i=1}^{N} N_i w_i$$

$$\theta_x=\sum_{i=1}^{N} N_i \theta_{x_i},\quad \theta_y=\sum_{i=1}^{N} N_i \theta_{y_i},\quad \theta_z=\sum_{i=1}^{N} N_i \theta_{z_i} \qquad (2)$$

where N is the number of nodes in the finite element. A nine-node Lagrangian element has been adopted in this work.

For each node, it is convenient to write the vector of unknowns as

$$\{q_i\}=\{u_i v_i w_i \theta_{x_i} \theta_{y_i} \theta_{z_i}\}^{\mathrm{T}}. \qquad (3)$$

The deformations are written as the summation of a linear plus a non-linear part, leading to

$$\{\epsilon\}=\{\epsilon_0\}+\{\epsilon_1\}$$

$$=\begin{Bmatrix} u_{,x} \\ v_{,y} \\ u_{,y}+v_{,x} \\ -\theta_{x,x} \\ -\theta_{y,y} \\ -\theta_{x,y}-\theta_{y,x} \\ w_{,y}-\theta_y \\ w_{,x}-\theta_x \\ \theta_z \end{Bmatrix}+\tfrac{1}{2}\begin{Bmatrix} v_{,x}^2+w_{,x}^2 \\ u_{,y}^2+w_{,y}^2 \\ 2w_{,x}w_{,y} \\ 0 \\ 0 \\ 0 \\ 0 \\ 0 \\ 0 \end{Bmatrix}. \qquad (4)$$

where

$$\{\epsilon\}=\{\epsilon_x \epsilon_y \gamma_{xy} \kappa_x \kappa_y \kappa_{xy} \gamma_{yz} \gamma_{zx} \theta_z\}^{\mathrm{T}} \qquad (5)$$

and ϵ_x, ϵ_y, and γ_{xy} are the in-plane strains, κ_x, κ_y and κ_{xy} are the curvatures, γ_{yz} and γ_{zx} are the out-of-plane shear strains and θ_z is the in-plane rotation.

Matrix $[B_0]$ employed in Ref. [14] results from the Mindlin–Reissner assumptions as

$$[B_0]=\begin{bmatrix} \frac{\partial N_i}{\partial x} & 0 & 0 & 0 & 0 & 0 \\ 0 & \frac{\partial N_i}{\partial y} & 0 & 0 & 0 & 0 \\ \frac{\partial N_i}{\partial y} & \frac{\partial N_i}{\partial x} & 0 & 0 & 0 & 0 \\ 0 & 0 & 0 & -\frac{\partial N_i}{\partial x} & 0 & 0 \\ 0 & 0 & 0 & 0 & -\frac{\partial N_i}{\partial y} & 0 \\ 0 & 0 & 0 & -\frac{\partial N_i}{\partial y} & -\frac{\partial N_i}{\partial x} & 0 \\ 0 & 0 & \frac{\partial N_i}{\partial y} & 0 & -N_i & 0 \\ 0 & 0 & \frac{\partial N_i}{\partial x} & -N_i & 0 & 0 \\ 0 & 0 & 0 & 0 & 0 & N_i \end{bmatrix}. \qquad (6)$$

The matrix $[B_1]$ is a function of the nodal displacements, i.e. $[B_1(q)]$. Following Zienkiewicz and Taylor [14] we can write the non-linear part of the strains as follows

$$\{\epsilon_1\}=\tfrac{1}{2}\begin{bmatrix} 0 & v_{,x} & w_{,x} & 0 \\ u_{,y} & 0 & 0 & w_{,y} \\ 0 & 0 & w_{,y} & w_{,x} \\ 0 & 0 & 0 & 0 \\ 0 & 0 & 0 & 0 \\ 0 & 0 & 0 & 0 \\ 0 & 0 & 0 & 0 \\ 0 & 0 & 0 & 0 \\ 0 & 0 & 0 & 0 \end{bmatrix}\begin{Bmatrix} u_{,y} \\ v_{,x} \\ w_{,x} \\ w_{,y} \end{Bmatrix}$$

$$=\tfrac{1}{2}[A][\theta]=[B_1(q)]\{q\} \qquad (7)$$

where the matrices $[A]$ and $[\theta]$ are still a function of the nodal displacements. Matrix $[\theta]$ can be written as

$$[\theta]=\begin{Bmatrix} u_{,y} \\ v_{,x} \\ w_{,x} \\ w_{,y} \end{Bmatrix}$$

$$=\begin{bmatrix} N_{1,y} & 0 & 0 & 0 & 0 & 0 & \dots \\ 0 & N_{1,x} & 0 & 0 & 0 & 0 & \dots \\ 0 & 0 & N_{1,x} & 0 & 0 & 0 & \dots \\ 0 & 0 & N_{1,y} & 0 & 0 & 0 & \dots \end{bmatrix}$$

$$\{q\}=[G]\{q\}. \qquad (8)$$

this case

Taking the variation of eqn (7) one has

$$\mathrm{d}\{\epsilon_1\} = \tfrac{1}{2}\mathrm{d}[A]\{\theta\} + \tfrac{1}{2}[A]\,\mathrm{d}\{\theta\}$$
$$= [A]\,\mathrm{d}\{\theta\} = [A][G]\,\mathrm{d}\{q\} \tag{9}$$

and hence, it follows by definition that

$$[2B_1] = [A][G]. \tag{10}$$

On the other hand, matrix $[A(q)]$ can be written as the product of two matrices, the first containing the derivatives of the shape functions and the second the nodal displacements, as

$$[A(q)] = \begin{bmatrix} 0 & N_{i,x} & N_{i,x} & 0 \\ N_{i,y} & 0 & 0 & N_{i,y} \\ 0 & 0 & N_{i,y} & N_{i,x} \\ 0 & 0 & 0 & 0 \\ 0 & 0 & 0 & 0 \\ 0 & 0 & 0 & 0 \\ 0 & 0 & 0 & 0 \\ 0 & 0 & 0 & 0 \\ 0 & 0 & 0 & 0 \end{bmatrix}$$
$$\times \begin{bmatrix} \{q\} & 0 & 0 & 0 \\ 0 & \{q\} & 0 & 0 \\ 0 & 0 & \{q\} & 0 \\ 0 & 0 & 0 & \{q\} \end{bmatrix}. \tag{11}$$

3. TOTAL POTENTIAL ENERGY

The total potential energy V of the plate subjected to in-plane and transverse loading is the summation of the strain energy U and the load potential Ω

$$V = \frac{1}{2}\int \{\sigma\}^{\mathrm{T}}\{\epsilon\}\,\mathrm{d}v - \Lambda\{a\}^{\mathrm{T}}\{f\}. \tag{12}$$

The load vector $\{f\}$ is assumed to be incremented by a single load factor Λ. The stress vector $\{\sigma\}$ is in this case

$$\{\sigma\} = \{N_x N_y N_{xy} M_x M_y M_{xy} Q_y Q_x M_z\}^{\mathrm{T}} \tag{13}$$

where N_x, N_y and N_{xy} are the in-plane stress resultants, M_x, M_y and M_{xy} are the moment resultants, Q_y and Q_x are the out-of-plane shear stress resultants and M_z is the in-plane moment. The constitutive law is

$$\{\sigma\} = [C]\{\epsilon\}. \tag{14}$$

For the case of a plate made of laminated composite material, the constitutive law simplifies to

$$\begin{Bmatrix} N_x \\ N_y \\ N_{xy} \\ M_x \\ M_y \\ M_{xy} \\ Q_y \\ Q_x \\ M_z \end{Bmatrix} = \begin{bmatrix} A_{11} & A_{12} & A_{16} & B_{11} & B_{12} & B_{16} & 0 & 0 & 0 \\ A_{12} & A_{22} & A_{26} & B_{12} & B_{22} & B_{26} & 0 & 0 & 0 \\ A_{16} & A_{26} & A_{66} & B_{16} & B_{26} & B_{66} & 0 & 0 & 0 \\ B_{11} & B_{12} & B_{16} & D_{11} & D_{12} & D_{16} & 0 & 0 & 0 \\ B_{12} & B_{22} & B_{26} & D_{12} & D_{22} & D_{26} & 0 & 0 & 0 \\ B_{16} & B_{26} & B_{66} & D_{16} & D_{26} & D_{66} & 0 & 0 & 0 \\ 0 & 0 & 0 & 0 & 0 & 0 & A_{44} & A_{45} & 0 \\ 0 & 0 & 0 & 0 & 0 & 0 & A_{45} & A_{55} & 0 \\ 0 & 0 & 0 & 0 & 0 & 0 & 0 & 0 & C^* \end{bmatrix} \begin{Bmatrix} \epsilon_x \\ \epsilon_y \\ \gamma_{xy} \\ \kappa_x \\ \kappa_y \\ \kappa_{xy} \\ \gamma_{yz} \\ \gamma_{zx} \\ \theta_z \end{Bmatrix} \tag{15}$$

where, A_{ij}, B_{ij} and D_{ij} are the plate stiffness properties as computed using the Classical Lamination Theory, and C^* is a very small number compared to the stiffness values, that corresponds to in-plane rotation θ_z [15].

Substituting eqn (14) into eqn (12), the strain energy results in terms of the strains. Furthermore, the substitution of eqn (15) into V leads to the expression of the energy W in terms of discrete generalized coordinates, as written in eqn (8) of Part I [1].

4. MATRICES REQUIRED FOR THE STABILITY ANALYSIS

As a first step, the linear fundamental path $\{q^F\}$ should be obtained. The stiffness matrix is needed, and can be formulated as

$$[K_0] = \int_V [B_0]^{\mathrm{T}}[C][B_0]\,\mathrm{d}v \tag{16}$$

$$[K_0]\{q^{\mathrm{F}}\} = \{P\} \tag{17}$$

with respect to $\{q^F\}$, to determine the pre-buckling solution. The second step is the detection of the critical states along the fundamental path. For this reason, it is necessary to compute the geometric stiffness matrix $[K_\sigma]$. This can be done as follows:

$$[K_\sigma] = \int_v [G]^{\mathrm{T}}\,\mathrm{d}[A]^{\mathrm{T}}\{\sigma\}\,\mathrm{d}v. \tag{18}$$

Following Zienkiewicz and Taylor [14], the stress vector $\{\sigma\}$ is rearranged in a matrix form as

$$[\sigma] = \begin{bmatrix} N_y & 0 & 0 & 0 \\ 0 & N_x & 0 & 0 \\ 0 & 0 & N_x & N_{xy} \\ 0 & 0 & N_{xy} & N_y \end{bmatrix} \tag{19}$$

and hence, the geometric stiffness matrix $[K_\sigma]$ can be computed as

$$[K_\sigma] = \int_v [G]^T[\sigma][G]\,dv. \tag{20}$$

The linear eigenvalue problem is

$$([K_0] - \Lambda[K_\sigma])\{x\} = 0. \tag{21}$$

The critical states are determined from eqn (21) (i.e. the critical load Λ^c and the corresponding eigenvector $\{x\}$).

Next, attention is given to the study of the post critical path passing through the bifurcation point. First, we must determine whether the bifurcation is symmetric or asymmetric. For that, it is necessary to compute the matrix $[D_1(x)]$ contracted by the eigenvector $\{x\}$. This can be written in terms of finite element matrices as

$$\begin{aligned}[D_1(x)] = \int_v \{&[2B_1^i(\delta_j)]^T[C][B_0 + 2\Lambda B_1(q^F)]\{x\} \\ &+ [2B_1(x)]^T[C][B_0 + 2\Lambda B_1(q^F)] \\ &+ [B_0 + 2\Lambda B_1(q^F)]^T[C][2B_1(x)]\}\,dv \end{aligned} \tag{22}$$

where δ_i is the Kroneker delta, with values $\delta_i = 1$ if $i = j$, and $\delta_i = 0$ if $i \neq j$. The matrix $[2B_1^i(\delta_j)]$ can be computed from the second matrix of eqn (11) if, instead of $\{q\}$, we insert a vector containing unit value in the jth row and zeros in the rest. The coefficient C may now be computed as

$$C = \{x\}^T D_1(x)\{x\}. \tag{23}$$

If $C = 0$, the critical state is a symmetric bifurcation, while for $C \neq 0$ the bifurcation is asymmetric. To follow the post buckling path, a perturbation analysis is carried out from the critical state. The variables a_i and Λ are expanded in terms of a perturbation parameter s, as indicated in eqn (18) of Part I [1]. In asymmetric bifurcation, the slope $\Lambda^{(1)C}$ of the post buckling path at the bifurcation point can be computed as

$$\Lambda^{(1)C} = -\frac{C}{2\{x\}^T[K_\sigma]\{x\}}. \tag{24}$$

The eigenvector $\{x\}$ can be normalized in several ways: one corresponds to $\{x\}^T[K_\sigma]\{x\} = 1$, so that the denominator in eqn (24) is 2. A second possibility is to choose a unit value for the largest component of $\{x\}$; this latter alternative has been implemented in the present work.

For linear fundamental path $\{a^{(1)C} \equiv \{x\}$. As a next step, the $\{a^{(2)C}\}$ coefficients are computed from

$$[K_T]\{a^{(2)C}\} = -([D_1(x)] + 2[K_\sigma]\Lambda^{(1)C})\{x\}^C \tag{25}$$

where the value of one of the components in the vector of the second derivatives of the displacements has to be chosen (i.e. $a_1^{(2)C} = 0$ if the perturbation parameter is q_1). Finally, the curvature of the post buckling path at the bifurcation point (for symmetric bifurcation) results in

$$\Lambda^{(2)C} = -\frac{\{x\}^T[D_2(x,x)]\{x\} + 3\{x\}^T[D_1(x)]\{a^{(2)C}\}}{3\{x\}^T[K_\sigma]\{x\}}. \tag{26}$$

The matrix $[D_2(x,x)]$ contracted by the $\{x\}$ eigenvector can be computed from

$$\begin{aligned}[D_2(x,x)] = \int_v \{&[2B_1^i(\delta_j)]^T[C][2B_1(x)]\{x\} \\ &+ 2[2B_1(x)]^T[C][2B_1(x)]\}\,dv. \end{aligned} \tag{27}$$

5. ORIENTATION OF A PLATE ELEMENT IN THE 3-D SPACE

The plate element described previously has been developed for plane applications. In the case of a three-dimensional structural geometry, a transformation needs to be performed on the nodal coordinates and nodal displacements.

The element surface can be clearly defined from the nodal coordinates. For an N-noded isoparametric element, one can write

$$x = \sum_{i=1}^{N} N_i x_i, \quad y = \sum_{i=1}^{N} N_i y_i, \quad z = \sum_{i=1}^{N} N_i z_i. \tag{28}$$

The element surface is a three-dimensional vector $\mathbf{r}$

$$\begin{aligned}\mathbf{r} &= x\hat{i} + y\hat{j} + z\hat{k} \\ &= \left(\sum_i N_i x_i\right)\hat{i} + \left(\sum_i N_i y_i\right)\hat{j} + \left(\sum_i N_i z_i\right)\hat{k}. \end{aligned} \tag{29}$$

Since the shape functions N_i are functions of ξ and η, the element surface is also a function of ξ and η

$$\mathbf{r} = \mathbf{r}(\xi, \eta). \tag{30}$$

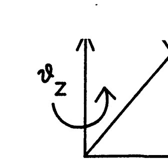

From vector analysis, the normal vector $\mathbf{n}_z$ on the element surface at a point (ξ_0, η_0) is

$$\mathbf{n}_z = \left(\frac{\partial \mathbf{r}}{\partial \xi}\right)_0 \times \left(\frac{\partial \mathbf{r}}{\partial \eta}\right)_0 \tag{31}$$

where

$$\mathbf{r}_{,\xi} = \left[\sum_i \left(\frac{\partial N_i}{\partial \xi}\right) x_i\right]\hat{i} + \left[\sum_i \left(\frac{\partial N_i}{\partial \xi}\right) y_i\right]\hat{j} + \left[\sum_i \left(\frac{\partial N_i}{\partial \xi}\right) z_i\right]\hat{k} \tag{32}$$

and

$$\mathbf{r}_{,\eta} = \left[\sum_i \left(\frac{\partial N_i}{\partial \eta}\right) x_i\right]\hat{i} + \left[\sum_i \left(\frac{\partial N_i}{\partial \eta}\right) y_i\right]\hat{j} + \left[\sum_i \left(\frac{\partial N_i}{\partial \eta}\right) z_i\right]\hat{k}. \tag{33}$$

Note that since the element is flat, we need to define the normal at only one point on the element surface. As soon as $\mathbf{n}_z$ is defined, an orthogonal coordinate system can be generated following the procedure described by Ahmad *et al.* [15], which follows.

First, a vector $\mathbf{n}_y$ is defined as $\mathbf{n}_y = \mathbf{n}_z \times \mathbf{i}$; and using $\mathbf{n}_y$, we define a vector $\mathbf{n}_x$ as $\mathbf{n}_x = \mathbf{n}_y \times \mathbf{n}_z$. The three vectors $\mathbf{n}_x$, $\mathbf{n}_y$ and $\mathbf{n}_z$ define an orthogonal coordinate system that is uniquely attached to the finite element.

As a second step, we normalize $\mathbf{n}_x$, $\mathbf{n}_y$ and $\mathbf{n}_z$ to $\mathbf{i}'$, $\mathbf{j}'$ and $\mathbf{k}'$, using

$$\hat{i}' = \frac{(n_x)_x}{\|n_x\|}\hat{i} + \frac{(n_x)_y}{\|n_x\|}\hat{j} + \frac{(n_x)_z}{\|n_x\|}\hat{k} \tag{34}$$

$$\hat{j}' = \frac{(n_y)_x}{\|n_y\|}\hat{i} + \frac{(n_y)_y}{\|n_y\|}\hat{j} + \frac{(n_y)_z}{\|n_y\|}\hat{k} \tag{35}$$

$$\hat{k}' = \frac{(n_z)_x}{\|n_z\|}\hat{i} + \frac{(n_z)_y}{\|n_z\|}\hat{j} + \frac{(n_z)_z}{\|n_z\|}\hat{k} \tag{36}$$

where for instance the norm for $\mathbf{n}_x$ is

$$\|n_x\| = \sqrt{(n_x)_x^2 + (n_x)_y^2 + (n_x)_z^2}. \tag{37}$$

The above procedure is not valid in the special case when the normal $\mathbf{n}_z$ is parallel to the unit vector $\mathbf{i}$. Then, we assign $\mathbf{n}_x = \mathbf{j}$ and we compute $\mathbf{n}_y = \mathbf{n}_z \times \mathbf{n}_x$. By writing in a matrix form,

$$\begin{Bmatrix} \hat{i}' \\ \hat{j}' \\ \hat{k}' \end{Bmatrix} = \begin{bmatrix} \lambda_{11} & \lambda_{12} & \lambda_{13} \\ \lambda_{21} & \lambda_{22} & \lambda_{23} \\ \lambda_{31} & \lambda_{32} & \lambda_{33} \end{bmatrix} \begin{Bmatrix} \hat{i} \\ \hat{j} \\ \hat{k} \end{Bmatrix} \tag{38}$$

we have the directional cosines (λ_{ij}) that define the transformation of coordinates from the old to the new (prime) coordinate system. Each component of λ matrix is the cosine of the angle between i and j', where i, $j = x$, y, z. This matrix will be used to transform the nodal coordinates and the displacement vectors of the element. The following relations can be immediately stated

$$\begin{Bmatrix} x_i' \\ y_i' \\ z_i' \end{Bmatrix} = \begin{bmatrix} \lambda_{11} & \lambda_{12} & \lambda_{13} \\ \lambda_{21} & \lambda_{22} & \lambda_{23} \\ \lambda_{31} & \lambda_{32} & \lambda_{33} \end{bmatrix} \begin{Bmatrix} x_i \\ y_i \\ z_i \end{Bmatrix} \tag{39}$$

and

$$\begin{Bmatrix} u_i' \\ v_i' \\ w_i' \end{Bmatrix} = \begin{bmatrix} \lambda_{11} & \lambda_{12} & \lambda_{13} \\ \lambda_{21} & \lambda_{22} & \lambda_{23} \\ \lambda_{31} & \lambda_{32} & \lambda_{33} \end{bmatrix} \begin{Bmatrix} u_i \\ v_i \\ z_i \end{Bmatrix} \tag{40}$$

The vectors of the rotations θ_x, θ_y and θ_z are oriented in a special way on the coordinate system (Fig. 2), and hence, special care must be paid for their transformation to another coordinate system. At first, the rotation vectors θ_x, θ_y and θ_z must be reoriented to θ_1, θ_2 and θ_3. This can be done as follows:

$$\{\theta^*\} = \begin{Bmatrix} \theta_1 \\ \theta_2 \\ \theta_3 \end{Bmatrix} = \begin{bmatrix} 0 & 1 & 0 \\ -1 & 0 & 0 \\ 0 & 0 & 1 \end{bmatrix} \begin{Bmatrix} \theta_x \\ \theta_y \\ \theta_z \end{Bmatrix} = [T]\{\theta\}. \tag{41}$$

Before and after multiplication of λ by $\mathbf{T}$ gives as a result the modified transformation matrix λ^* for the rotation vectors, which is

$$\{\lambda^*\} = \begin{bmatrix} \lambda_{22} & -\lambda_{12} & -\lambda_{32} \\ -\lambda_{21} & \lambda_{11} & \lambda_{31} \\ -\lambda_{23} & \lambda_{13} & \lambda_{33} \end{bmatrix} \tag{42}$$

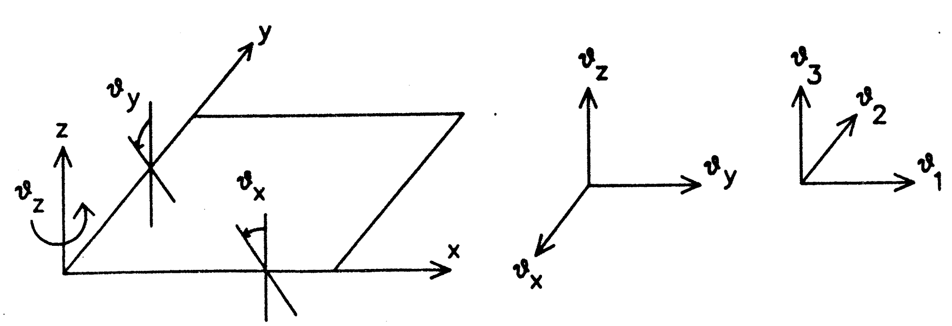

Fig. 2. Transformation procedure for θ_x, θ_y and θ_z.

hence, the displacement transformation matrix for each node of the element, from a system of axes to a prime system of axes, is

$$[\Lambda]_i = \begin{bmatrix} [\lambda]_i & [0] \\ [0] & [\lambda^*]_i \end{bmatrix}, \quad i = 1, \ldots, N. \tag{43}$$

6. RESULTS FOR PLATES AND PLATE ASSEMBLIES

The procedure described previously, has been applied for the development of shear deformable plate element capable of representing the buckled configuration of a plate or plate assembly. For specific examples discussed herein, a critical state along the fundamental path has been detected and the nature of the bifurcation has been studied. It is not easy to find examples of post buckling analysis of composite thin walled elements in the literature, and only a limited number of problems have been employed for validation of the present code.

Composite plate

Let us first consider the case of a rectangular composite plate subjected to inplane axial compression. The geometry and the loading are shown in Fig. 3. The material properties with reference to eqn (15) are $A_{11} = 1,017{,}650$ lb in^{-1}, $A_{22} = 391{,}404$ lb in^{-1}, $A_{12} = 129{,}187.5$ lb in^{-1}, $A_{66} = 159{,}375$ lb in^{-1}, $D_{11} = 11{,}925.58$ lb in, $D_{22} = 4586.76$ lb in, $D_{12} = 1513.91$ lb in, $D_{66} = 1867.67$ lb in, and $A_{44} = A_{55} = 132{,}187.5$ lb in^{-1}, where $B_{ij} = 0$ for $i, j = 1, 2, 6$, $A_{45} = A_{54} = 0$ and C^* is a very small number compared to A_{ij} stiffnesses. The plate is simply supported at all edges. A finite element mesh of 16 elements has been formulated, and the lowest critical load has found to be $\Lambda^C = 1943$ lb in^{-1} and associated with one buckling half wave. The nature of the bifurcation is stable symmetric, and the curvature of the post buckling path at the bifurcation point has been found to be $\Lambda^{(2)C} = 4361.4$ lb in^{-3}. The critical load was computed by Pandey [16] as $\Lambda^C = 1949$ lb in^{-1}, also associated with one buckling half wave. From the results of Pandey, the nature of the bifurcation is again stable symmetric, and the curvature of the post buckling path at the bifurcation point is $\Lambda^{(2)C} = 6283.4$ lb in^{-3}. Hence, the model is in a good agreement regarding the critical buckling load values.

The difference in the values of the curvature of the post buckling path is due to the fact that finite element model allows for inplane waviness in the buckled configuration, while Pandey's model assumes the ends to remain straight after buckling. This case is thoroughly discussed in Ref. [6] for a steel square plate.

Also, a clamped circular steel plate subjected to inplane compression has been studied in post buckling. The bifurcation in this case is also stable symmetric, and the critical load and curvature have been computed as $\Lambda^C = 405.6$ lb in^{-1} and $\Lambda^{(2)C} = 15{,}768$ lb in^{-3}, respectively. According to Thompson and Hunt [2] the critical load and curvature are $\Lambda^C = 403.3$ lb in^{-1} and $\Lambda^{(2)C} = 16530$ lb in^{-3}, respectively. There is a difference of 4.8% in the value of the curvature between the numerical and analytical solution due to the mesh.

Clamped I-beam

As a second case let us consider a wide flange I-beam that has been studied by Vakiener *et al.* [17]. The cross sectional dimensions are 8 × 8 in and the thickness of the flanges and the web is 3/8 in. The length of the column is 5 ft (60 in). Vakiener *et al.* [17] report apparent (homogenized) material properties, that in terms of engineering constants are $E_1 = 2600$ ksi, $E_2 = 1000$ ksi, $G_{12} = 425$ ksi, $\nu_{12} = 0.33$ and $\nu_{21} = 0.127$. The stiffness data as required by eqn 15, can be computed using the classical lamination theory [18]. Both ends are assumed simply supported. More specifically, the boundary conditions are determined as follows:

(1) lateral deflection is restrained in both planes (x and y, x and z) at both ends;

(2) longitudinal deflection is restrained at one end but it is unrestrained at the other end where the load is applied;

(3) torsional rotation is restrained at both ends;

(4) flexural rotation is allowed at both ends of the section.

The applied load in this case is uniformly distributed over the flanges and the web, while in Vakiener *et al.* [17] the nodes at the free edge of the flange receive one-third of the load applied to the node at the junction of flange and web, and the nodes along

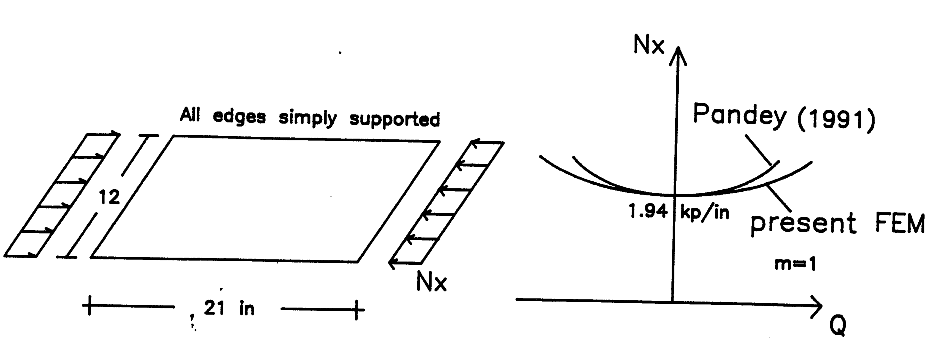

Fig. 3. Orthotropic plate under inplane compression.

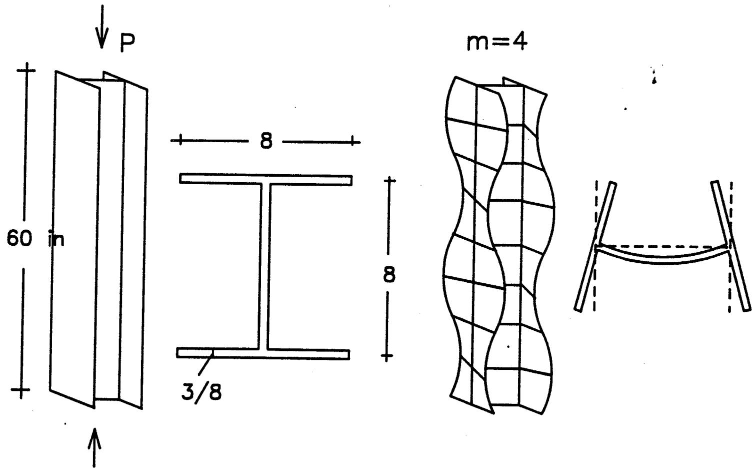

Fig. 4. Local buckling of an orthotropic I-beam under axial compression.

the interior of the flange and web receive two-thirds of the load applied to the node at the flange-web junction. The critical buckling load computed in Vakiener *et al.* [17] for a 1440 element mesh is $\Lambda^C = 58$ kips corresponding to four buckling half waves along the length. The present model with 25 elements predicts a critical load $\Lambda^C = 55.5$ kips corresponding again to four buckling half waves. The results are in a good agreement, despite the difference in the loading systems considered. Furthermore, the nature of the bifurcation has been found to be stable symmetric and the curvature of the post buckling path at the critical state has been computed as $\Lambda^{(2)C} = 242.93$ kip in^{-2} (see Fig. 4). A stable post critical path is consistent with the fact that Vakiener *et al.* [17] were able to carry the column buckling experiment into the post buckling regime. However, they do not report any post buckling analysis.

Simply-supported I-column

The stability of an FRP composite I-beam subjected to pinned end compression is also considered. More specifically, a $6 \times 6 \times \frac{1}{4}$ I-column made from E-glass fiber reinforced vinylester is studied next (Creative Pultrusions [19]). The length of the column is 100 in. The material properties for the flanges are $A_{11} = 893{,}500$ lb in^{-1}, $A_{22} = 343{,}000$ lb in^{-1}, $A_{12} = 130{,}800$ lb in^{-1}, $A_{66} = 113{,}600$ lb in^{-1}, $D_{11} = 4289$ lb in, $D_{22} = 2029$ lb in, $D_{12} = 807.3$ lb in, $D_{66} = 641.5$ lb in, and $A_{44} = A_{55} = 94{,}666$ lb in^{-1}, where $B_{ij} = 0$ for $i, j = 1, 2, 6$, $A_{45} = A_{54} = 0$ and $C^* \approx 0$; and for the web $D_{11} = 4090$ lb in, $D_{22} = 1863$ lb in, $D_{12} = 731.6$ lb in, $D_{66} = 596.1$ lb in.

The boundary conditions as applied in the previous example do not allow for global buckling. The new consideration in this case is that the ends of the flanges have no restraint whatsoever and only the ends of the web are restrained as in the previous example. These boundary conditions now allow for Euler buckling about the weak axis of the cross-section. Local buckling occurs for $\Lambda^C = 27{,}324$ lb and the post buckling path is stable symmetric and the curvature has found to be $\Lambda^{(2)C} = 172{,}182$ lb in^{-2}. Global buckling occurs for $\Lambda^C = 29{,}762$ lb and the post buckling path is also stable symmetric with the curvature in this case given by $\Lambda^{(2)C} = 27.3$ lb in^{-2}. The two post critical equilibrium paths are plotted in Fig. 5 in terms of the applied load.

Angle section

Next, the stability of an angle section FRP bar has been studied. It is a $6 \times 6 \times \frac{3}{8}$ in and 20 in long bar, that is subjected to uniformly distributed axial compression applied at the ends. The material properties are $A_{11} = 1{,}284{,}000$ lb in^{-1}, $A_{22} = 480{,}300$ lb in^{-1}, $A_{12} = 180{,}800$ lb in^{-1}, $A_{66} = 160{,}800$ lb in^{-1}, $D_{11} = 13{,}910$ lb in, $D_{22} = 6082$ lb in, $D_{12} = 2364$ lb in, $D_{66} = 1968$ lb in, and $A_{44} = A_{55} = 134{,}000$ lb in^{-1}. The boundary conditions applied are the same as in the clamped I-beam case; that is we are mainly concerned with local buckling and it is assumed that other forms of instability such as Euler

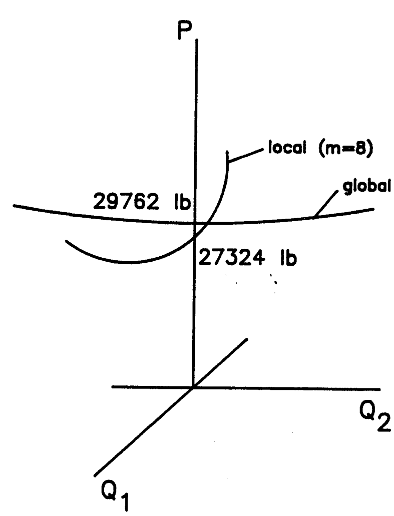

Fig. 5. Global and local buckling of an FRP I-beam under axial compression.

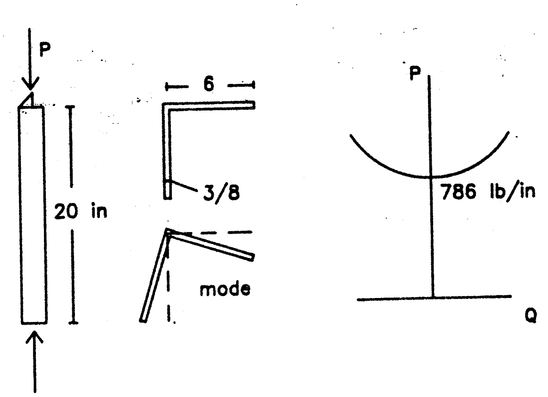

Fig. 6. Geometry and buckling of an FRP angle section.

buckling are prevented from occurring. The stability analysis using finite elements determined a critical buckling load $\Lambda^C = 786$ lb in^{-1}. The nature of the bifurcation is stable and symmetric, and the curvature of the post buckling path at the bifurcation point has been found to be $\Lambda^{(2)C} = 1035$ lb in^{-3}. The mode corresponding to the critical load is axial–torsional. The geometry of the angle section, the critical load and the post buckling path and modal shape can be seen in Fig. 6.

Unicolumn

As a final example, the buckling behavior of a composite box–beam with flanges called unicolumn (see Fig. 7) has been studied. The cross-sectional shape is 12-by-12 in with all walls having 5/16 in thickness and the length is 60 in. Experimental results for this shape have been presented by Yuan *et al.* [20]. The unicolumn was designed to achieve higher capacity in carrying axial compressive loads and to facilitate construction by providing a convenient way to attach beams to the flanges of the unicolumn. The material properties presently used are $A_{11} =$ 808.66 kips in^{-1}, $A_{22} = 194.20$ kips in^{-1}, $A_{12} = 49.05$ kips in^{-1}, $A_{66} = 77.03$ kips in^{-1}, $B_{11} = -4.449$ kips, $B_{22} = -0.283$ kips, $B_{12} = -0.087$ kips, $B_{66} = -0.118$ kips, $D_{11} = 5.6671$ kips in, $D_{22} = 1.5223$ kips in, $D_{12} = 0.3814$ kips in, $D_{66} = 0.6026$ kips in, and $A_{44} = A_{55} = 64.19$ kips in^{-1}, not necessarily representative of current unicolumn sections. The load is uniformly distributed on the ends, and the boundary conditions applied are the same as in the case of the clamped I-beam. From the stability analysis, the critical buckling load has found to be $\Lambda^C = 1.7638$ kips in^{-1} associated with five half waves along the length. The modal shape is presented in Fig. 7. The bifurcation is in this case stable symmetric, with the curvature of the post critical path at the bifurcation point being $\Lambda^{(2)C} = 22.9$ kips in^{-3}. It is worth mentioning that the ultimate compressive load determined in the present analysis is 84.66 kips. Yuan *et al.* [20] reported higher ultimate loads for the unicolumn due to the different properties that correspond to the specimens. Note that a stable post critical path is consistent with the experiments by Yuan *et al.* [20] that were carried into the post critical regime. The post buckling path is also presented in Fig. 7.

For the unicolumn, a parametric study has been also performed to understand the influence of the geometry on the critical loads. More specifically, the width of the flanges b_2 (Fig. 7) varies from $b_2 = 0$ (square 6 × 6 in box-beam) to $b_2 = 3$ in (current unicolumn). The width of the box-section walls is $b_1 = 6$ in. The critical buckling load of each case is plotted vs the width ratio b_2/b_1 in Fig. 8. As a second case, the thickness t of the walls of the cross-section varies from $t = 5/32$ in to $t = 5/8$ in, while the dimensions of the cross-section are fixed to 12 × 12 in and $b_2 = 3$ in. The critical load is now plotted vs the ratio t/b_1 in Fig. 8. Notice that there is a maximum in P_{cr}

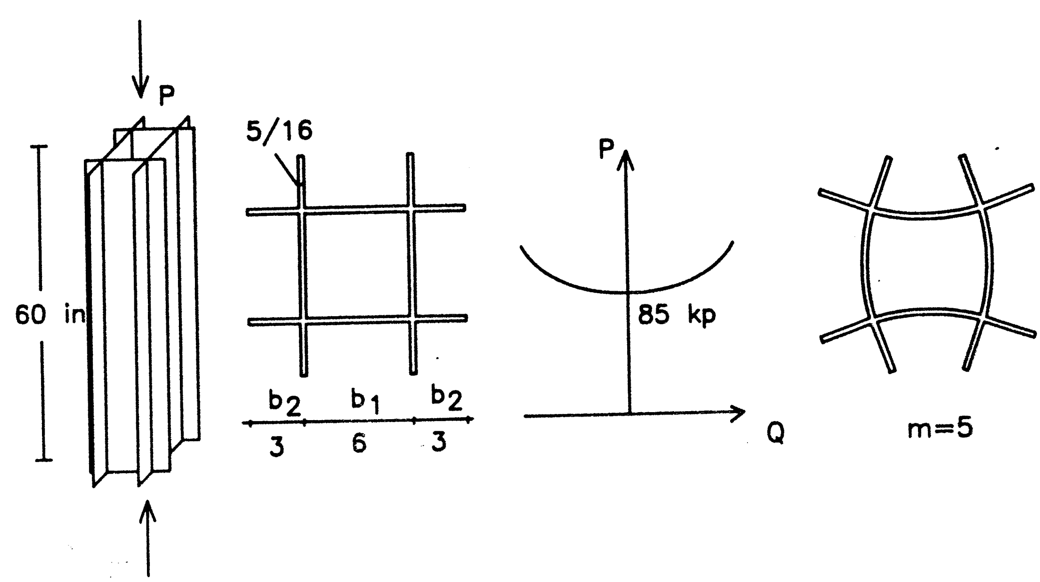

Fig. 7. Local buckling of a composite box-beam with flanges.

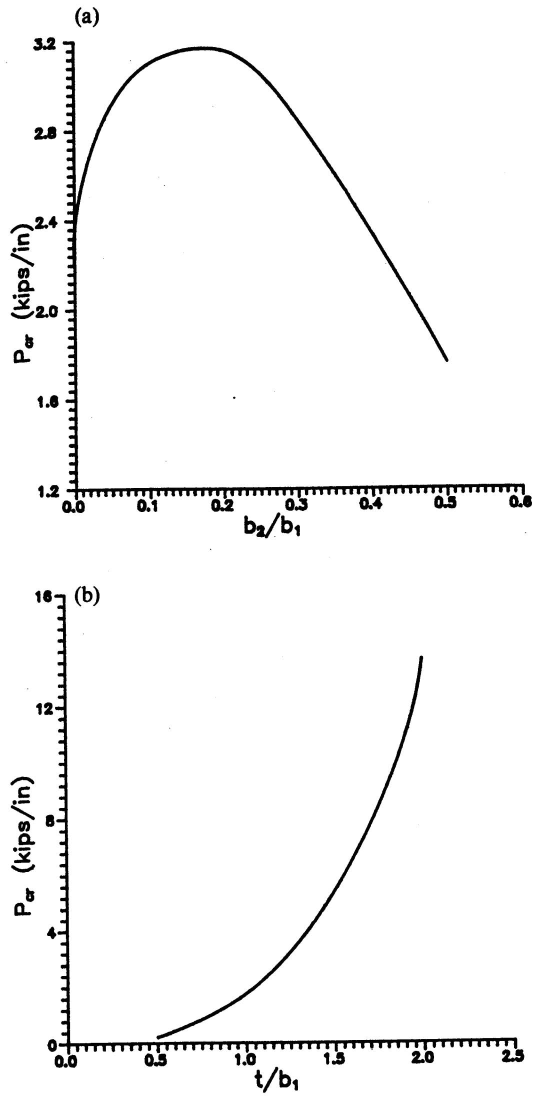

Fig. 8. Parametric study of local buckling loads.

for a ratio b_2/b_1 of about 0.175; this means that increasing the width of the flanges b_2 more than a given value (an optimum) does not lead to any improvement in the buckling load capacity of the unicolumn.

7. CONCLUSIONS

The finite element method has been employed for the post buckling analysis of plates and plate assemblies, like I-columns, angle section bars, and more complex cross-sectional shapes (unicolumn). The framework of the analysis is the general theory of elastic stability implemented into finite element analysis.

The main characteristics concerning the structures studied here are uniform compression at the ends of the plates or columns; simply supported or clamped boundary conditions; and that the flanges and the webs can freely expand in transverse direction to the applied load. The buckling modes as they come as a solution to an eigenvalue problem, may have in-plane waviness and amplitude modulation [21]. This may result in numerical differences between the finite element solution and analytical or semi-analytical solutions previously developed. In the present work, a nine-node Lagrangian element with 6 d.o.f. per node has been used; it requires 15 coefficients to model the properties of the composite material of each element, namely A_{11}, A_{22}, A_{12}, A_{66}, B_{11}, B_{22}, B_{12}, B_{66}, D_{11}, D_{22}, D_{12}, D_{66}, A_{44}, A_{55} and A_{45}. The fundamental path is linear, and the lowest value of critical load of the eigenvalue problem is considered for post buckling analysis. The general theory of elastic stability [2] has been successfully applied to plate and plate assemblies experiencing a bifurcation. The nature of the bifurcation that governs the post buckling behavior of the structure is determined. The slope and the curvature of the post buckling path at the bifurcation point is needed in order to follow the post buckling path up to point. Also, in the case of unstable symmetric or asymmetric bifurcation an imperfection sensitivity analysis can be performed and safety factors can be realistically determined. Since there is limited previous work in this field reported in the literature, numerical validation was performed for some of the cases considered. It is expected to further validate these results against new experimental work.

Concerning the application to composite materials, it is possible to say that the model developed here takes into account any kind of laminates and also plate assemblies and cross-sectional shapes of any geometrial complexity. Finite elements can easily take into account complex boundary conditions and loading. The accuracy of the results can be improved with mesh refinement. Thus, it is expected that it could be used as a useful tool mainly for the design of pultruted columns.

REFERENCES

1. L. Godoy, E. Barbero and I. Raftoyiannis, Finite elements for post-buckling analysis. I—The *W*-Formulation. *Comput. Struct.* **56**, 1009–1017 (1995).
2. J. M. Thompson and G. W. Hunt, *A General Theory of Elastic Stability*. Wiley, New York (1973).
3. A. C. Walker, The post-buckling behavior of simply supported square plates. *Aero. Q.* **XX**, 203–22 (1969).
4. F. Flores, and L. Godoy, Elastic postbuckling analysis via finite element and perturbation techniques, Part I: Formulation. *Int. J. numer. Meth. Engng* **33**, 1775–1794 (1992).
5. L. A. Godoy, Finite strip methods for instability of prismatic plate assemblies. *Engng Anal.* **5**(2), 100–107 (1988).
6. T. R. Graves Smith and S. Sridharan, A finite strip method for the post-locally buckled analysis of plate structures. *Int. J. mech. Sci.* **20**, 833–842 (1978).
7. S. Sridharan and T. R. Graves Smith, Postbuckling analyses with finite strips. *J. Engng Mech. Div. ASCE* **107**, EM5, 869–888 (1981).
8. S. Sridharan, A finite strip analysis of locally buckled plate structures subject to non-uniform compression. *Engng Struct.* **4**, 249–255 (1982).

9. S. Sridharan, A semi-analytical method for the post-local-torsional buckling analysis of prismatic plate structures. *Int. J. numer. Meth. Engng* **18**, 1685–97 (1982).
10. M. Zeggane and S. Sridharan, Stability analysis of long laminate composite plates using Reissner–Mindlin "infinite" strips. *Comput. Struct.* **40**(4), 1033–1042 (1991).
11. M. Zeggane and S. Sridharan, Buckling under combined loading of shear deformable laminated anisotropic plates using "infinite" strips. *Int. J. numer. Meth. Engng*. **31,** 1319–1331 (1991).
12. D. J. Dawe, Letter to the editor, Buckling under combined loading, of shear deformable laminated anisotropic plates using "infinite" strips [M. Zeggane and S. Sridharan, *Int. J. numer. Meth. Engng*. **31,** 1319–1331 (1991)], **35,** 1347–1349 (1992).
13. S. Sridharan, M. Zeggane, and S. Starnes, Mode interaction in stiffened composite panels. *First Joint Meeting SES-ASCE-ASME*, Charlottesville, VA, 6–9 June (1993).
14. O. C. Zienkiewicz, and R. L. Taylor, *The Finite Element Method.* 4th Edn. McGraw-Hill, London (1991).
15. S. Ahmad, B. M. Irons, and O. C. Zienkiewicz, A simple matrix-vector handling scheme for three-dimensional and shell analysis. *Int. J. numer. Meth. Engng* **2,** 509–522 (1970).
16. M. D. Pandey, Structure–material interaction in stability of fibrous composite elements. Ph. D. Thesis, University of Waterloo (1991).
17. A. R. Vakiener, A. Zureick and K. M. Will, Prediction of local flange buckling in pultruted shapes by finite element analysis. In *Advanced Composite Materials in Civil Engineering Structures* (Edited by S. L. Iyer), pp. 302–312. ASCE, New York (1991).
18. S. W. Tsai, *Composites Design*, 4th Edn. Think Composites, New York, (1989).
19. Creative Pultrusions Inc, *Design Guide*. Alum Bank, PA (1989).
20. R. L. Yuan, Z. Hasen, A. Green and T. Bisarnsin, Fiber-reinforced plastic composite columns. In *Advanced Composite Materials in Civil Engineering Structures* (Edited by S. L. Iyer), pp. 205–211. ASCE, New York (1991).
21. W. T. Koiter, General theory of mode interaction in stiffened plate and shell structures. Report No. 590, Delft University of Technology (1976).